

<https://doi.org/10.1038/s42003-025-08168-8>

# Selective serotonin reuptake inhibitors induce cardiac toxicity through dysfunction of mitochondria and sarcomeres



Yawei Shen<sup>1,2,3</sup>, Cameron E. Brown<sup>1,2</sup>, Xiao Li<sup>1,2</sup>, Peng Zhang<sup>1</sup>, Stacey R. McGee<sup>4</sup>, Søren C. Spina<sup>1</sup>, J. Ricardo Loret de Mola<sup>5</sup>, Joanna L. Fiddler<sup>6</sup>, Haodi Wu<sup>7</sup> & Qing Liu<sup>1,2</sup> ✉

The administration of selective serotonin reuptake inhibitors (SSRIs) during pregnancy can increase the odds of congenital heart defects in babies. The present study aims to explore the toxic effects of SSRIs on the cardiac systems and the underlying mechanism. We apply human pluripotent stem cells to establish 2D-monolayer cardiomyocyte and 3D-cardiac organoid models to evaluate the effects of three SSRIs (fluoxetine, paroxetine, and sertraline) on cardiac development. We observe that SSRIs exposure inhibited ATP production and mitochondrial respiration and disrupted mitochondrial homeostasis and sarcomere structure in the differentiating cardiomyocytes, presenting high risks of dysfunction and abnormality of cardiomyocytes. Further analyses in the cardiac organoid model show that SSRIs not only reduce mitochondrial respiration and ATP production, but may also affect cardiac development and angiogenesis. Altogether, our study reveals that SSRIs induce mitochondrial dysfunction and sarcomeric disorganization in cardiomyocytes, implying their potential risk to the cardiac system.

Selective serotonin reuptake inhibitors (SSRIs) are the most prescribed class of medications for the treatment of depression. SSRIs increase the levels of serotonin (5-hydroxytryptamine or 5-HT) by inhibiting serotonin transporter at the presynaptic axon terminal. It allows serotonin to remain in the synaptic cleft and stimulates postsynaptic receptors for a longer period to alleviate depressive symptoms in depressed patients<sup>1–3</sup>. SSRIs have been commonly used by women during their pregnancy. The prevalence rates of SSRIs administration during pregnancy have increased fourfold between 1996 and 2005, with the recent estimated international prevalence of 3% and the US prevalence of 6%<sup>4–6</sup>.

SSRIs have been found to exert adverse effects in adults and during early development in infants or utero. SSRIs were reported to cause platelet adhesion and aggregation, cardiovascular side effects, gastrointestinal side effects, hepatotoxicity, seizure, weight gain, dry mouth, hyponatremia, sleep, and sweating<sup>7</sup>. In the cardiovascular system, SSRIs were reported to cause arrhythmias, syncope, increased right ventricular volume, atrial fibrillation,

bradycardia, and the production of proinflammatory cytokines leading to atherosclerotic development<sup>8,9</sup>. In addition, about 30% of babies whose mothers had taken SSRIs while pregnant experienced neonatal adaptation syndrome, which can cause irritability, abnormal crying, tremor, jitteriness, lethargy, respiratory distress, poor muscle tone, and, rarely, convulsions<sup>10–12</sup>. The use of some SSRIs during the first trimester has been identified as increasing the odds of congenital heart defects<sup>13</sup>. SSRIs and their metabolites can cross the placental barrier into the fetal blood<sup>14</sup>. Therefore, SSRIs may pose risks of heart toxicity in the fetuses of patients taking SSRIs during pregnancy.

We utilized human pluripotent stem cells (hPSCs) to generate both 2-dimensional (2D-) monolayer cardiomyocytes and 3-dimensional (3D-) cardiac organoids models to evaluate the potential cardiotoxic effects of SSRIs. Compared to animal models, hPSCs avoid species-specific impacts that may arise during the use of non-human model organisms. Monolayer cardiomyocytes derived from hPSCs have been widely used for disease

<sup>1</sup>Department of Biological Sciences, Clemson University, Clemson, SC, USA. <sup>2</sup>Center for Human Genetics, Clemson University, Greenwood, SC, 29646, USA.

<sup>3</sup>College of Fisheries, Henan Normal University, Xinxiang, 453007 Henan, China. <sup>4</sup>Department of Physiology, Southern Illinois University School of Medicine,

Carbondale, IL, USA. <sup>5</sup>Department of Obstetrics and Gynecology, Southern Illinois University School of Medicine, Springfield, IL, USA. <sup>6</sup>Department of Food, Nutrition, and Packaging Sciences, Clemson University, Clemson, SC, 29634, USA. <sup>7</sup>Heart, Lung, Blood, and Vascular Medicine Institute, Department of Medicine, Division of Cardiology, University of Pittsburgh, Pittsburgh, PA, USA. ✉e-mail: [qliu4@clemson.edu](mailto:qliu4@clemson.edu)

modeling and pharmacologic evaluation<sup>15</sup>. More recently, the development of 3D-cardiac organoids has been rapidly used as an emerging technology to better understand early heart development. It has been shown that the differentiated cardiac organoids can recapitulate patterns of early cardiogenesis, including myocardial layer, foregut endoderm anlagen, vessel-like structures, and endocardial-like cells<sup>16–18</sup>. Cardiomyocytes and cardiac organoids are derived from human pluripotent stem cells, thus, presenting ideal models for the studies of cardiac development, cardiac diseases, drug screening, and cellular therapies<sup>19,20</sup>.

In the present study, we evaluated the impacts of three SSRIs (fluoxetine, sertraline, and paroxetine) in the differentiated cardiomyocytes at their reported clinical levels<sup>21</sup>. We also investigated the long-term effects of SSRIs exposure during cardiac differentiation to mimic developmental exposure during early heart development. Functional genomics was implemented to understand mechanisms underlying SSRIs induced adverse impacts in both cardiomyocytes and cardiac organoids.

## Results

### SSRIs toxicity on differentiated cardiomyocytes

We evaluated the toxicity of three SSRIs (i.e., fluoxetine, paroxetine, and sertraline) in differentiated cardiomyocytes derived from both H1-human embryonic stem cells (H1-hESCs) and human induced

pluripotent stem cells (hiPSCs) (Fig. 1a). Based on the dose-response experiments, we found that the estimated lethal concentration 50 (LC<sub>50</sub>) levels in H1-CMs were 7.5  $\mu$ M (sertraline), 8.9  $\mu$ M (paroxetine), and 33.7  $\mu$ M (fluoxetine), and the estimated LC<sub>50</sub> levels in hiPS-CMs were 7.8  $\mu$ M (sertraline), 11.7  $\mu$ M (paroxetine), and 32.9  $\mu$ M (fluoxetine) (Fig. 1b, c). This demonstrates that sertraline exerts the highest toxicity in the differentiated cardiomyocytes compared to paroxetine and fluoxetine, despite variations in concentrations for cellular mortalities between different lines. To better evaluate the toxicity at clinical levels, H1-CMs and hiPS-CMs were exposed to the reported levels of SSRIs in patients' blood with concentrations of 30 nM (sertraline), 55 nM (paroxetine), and 263 nM (fluoxetine). Exposure to SSRIs at these concentrations for five days elevated intracellular levels of reactive oxygen species (ROS) and significantly reduced ATP production in the differentiated H1-CMs (Fig. 1d–g). However, SSRIs did not cause significant changes in ATP production after 24 hours of exposure (Supplementary Fig. 1). Using an Agilent Seahorse XF Analyzer, we measured the oxygen consumption rate (OCR) and further confirmed that mitochondrial basal and maximal respiration were decreased after exposure to clinical concentration levels of SSRIs over five days (Fig. 1h–j). However, spare respiration capacity was only reduced in the fluoxetine group, and ATP production was decreased in the paroxetine and sertraline groups (Fig. 1k–l). These

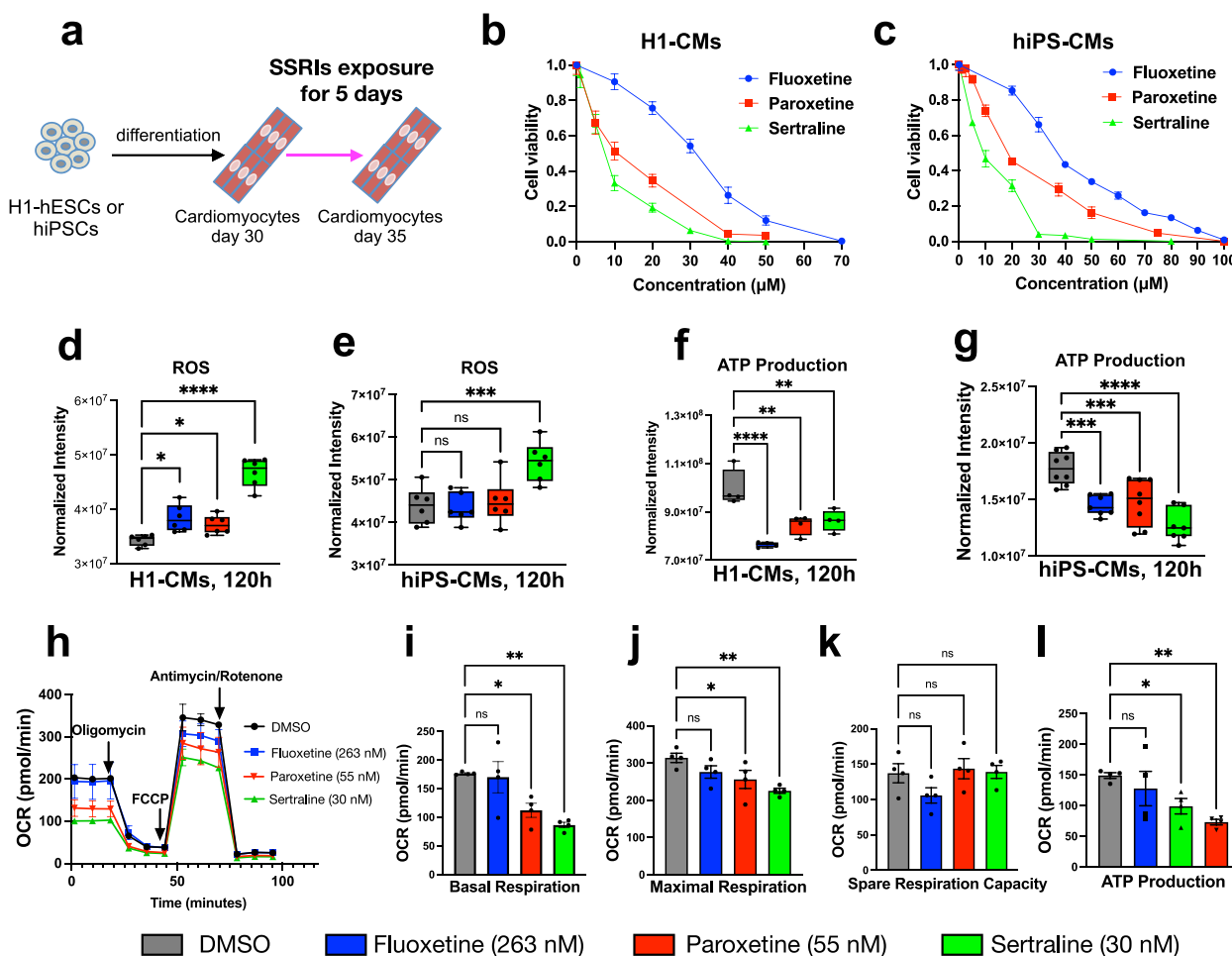


**Fig. 1 | SSRIs toxicity on differentiated cardiomyocytes.** **a** The procedure of SSRIs treatment on differentiated cardiomyocytes. The LC<sub>50</sub> levels of SSRIs toxicity on differentiated cardiomyocytes of H1-CMs (**b**) and hiPS-CMs (**c**). The ROS levels of differentiated H1-CMs (**d**) and hiPS-CMs (**e**) after five days of SSRIs exposure.  $n = 6$  biological replicates of each group for (**b–e**). The ATP production of differentiated H1-CMs (**f**) and hiPS-CMs (**g**) after five days of SSRIs exposure. ATP production was assessed using  $n = 4$  and  $n = 8$  biological replicates per group for H1-CMs and

hiPS-CMs, respectively. **h–l** The mitochondrial respiration levels of differentiated H1-CMs after five days of SSRIs exposure. **h** Graphical representation of the mitochondrial stress test, **i** basal respiration, **j** maximal respiration, **k** spare respiration capacity, **l** ATP-linked respiration. \* indicates  $p < 0.05$ , \*\* indicates  $p < 0.01$ , \*\*\* indicates  $p < 0.001$ , \*\*\*\* indicates  $p < 0.0001$ , ns indicates no significance.  $n = 4$  biological replicates of each group for (**h–l**).

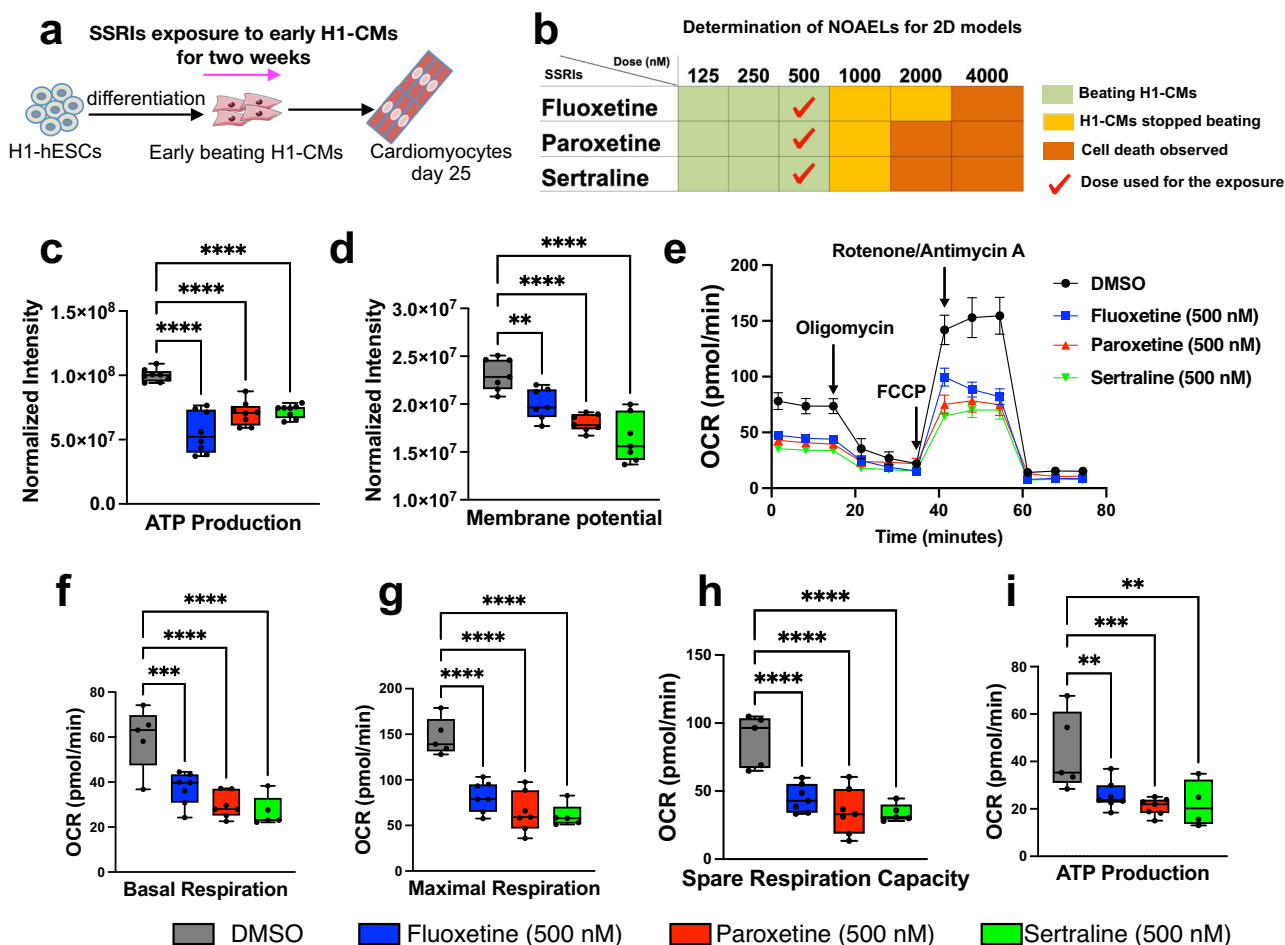


**Fig. 2 | SSRIs toxicity on differentiating cardiomyocytes.** **a** The procedure of SSRIs treatment on differentiating cardiomyocytes. **b** The identification of NOAEL of three SSRIs during the entire differentiation process of H1-CMs. **c** The ATP production of differentiating H1-CMs after SSRIs exposure ( $n = 8$  biological replicates). **d** The mitochondrial membrane potential of differentiating H1-CMs after SSRIs exposure ( $n = 7$  biological replicates). **e–i** The mitochondrial respiration

levels of differentiating H1-CMs after SSRIs exposure. **e** Graphical representation of the mitochondrial stress test. **f** basal respiration, **g** maximal respiration, **h** spare respiration capacity, **i** ATP respiration. \*indicates  $p < 0.05$ , \*\*indicates  $p < 0.01$ , \*\*\*indicates  $p < 0.001$ , \*\*\*\*indicates  $p < 0.0001$ .  $n = 5$  biological replicates for DMSO and Sertraline groups;  $n = 7$  for Fluoxetine and Paroxetine groups.

results suggested that long-term exposure to SSRIs at their clinical concentration levels decreased mitochondrial respiration and ATP production. However, the morphology of mitochondria (branch length and branches per network) and sarcomere (length and organization score) did not show significant changes after differentiated H1-CMs exposure to SSRIs for five days (Supplementary Fig. 2). Therefore, in subsequent experiments, we used the no-observed-adverse-effect level (NOAEL) to study the potential toxicity of SSRIs and underlying mechanisms in the cardiac system. The NOAEL of SSRIs in this study was the exposure concentration at which cardiomyocytes stop beating.

### SSRIs toxicity on developmental 2D-monolayer cardiomyocytes

To investigate their developmental toxicity during differentiation, we applied a 2D-monolayer cardiomyocyte differentiation model in this study. First, we identified the NOAEL of three SSRIs during the entire differentiation process (Fig. 2a), and we determined 500 nM as the NOAEL for all three SSRIs (Fig. 2b). We found that 500 nM of the three SSRIs can inhibit ATP production and mitochondrial membrane potential (Fig. 2c, d). We also observed that mitochondrial respiration was impaired upon exposure to 500 nM of SSRIs, including impaired mitochondrial basal and maximal respiration, and decreased spare respiration capacity and ATP production (Fig. 2e–i). These results suggested that SSRIs induced mitochondrial dysfunction and lower ATP production in developmental cardiomyocytes.

### SSRIs cause mitochondrial and sarcomeric disorganization of the cardiomyocytes

By examining mitochondrial morphology after two weeks of exposure to SSRIs, the differentiating H1-CMs exhibited smaller mitochondria branch lengths and decreased branches per network compared to the control group (Fig. 3a, c–d). The result suggested that long-term exposure to SSRIs disrupted mitochondrial homeostasis. Moreover, we examined the structural integrity of the cells with sarcomere structure by immunofluorescence staining (Fig. 3b). Our results show that sarcomere length was decreased only in the paroxetine group, and sarcomere organization score was significantly reduced in all exposure groups (Fig. 3e, f), indicating disarrangement of sarcomere structure after SSRIs exposure.

### Transcriptome profiling revealed distinct biological processes related to SSRIs toxicity in the 2D model

The RNA-seq analysis revealed that three SSRIs exhibited certain differences in the transcriptome. Principal component analysis (PCA) and inter-sample correlation revealed similar expression patterns and clustering in replicate samples (Fig. 4a). The expression profiles of differentially expressed genes (DEGs) were extracted and displayed by clustering heatmaps, showing significant differences in the comparison groups (Fig. 4b). We identified 163 DEGs in the fluoxetine group, 343 DEGs in the paroxetine group, and 306 DEGs in the sertraline group compared to the control group. Notably, only 31 DEGs are shared



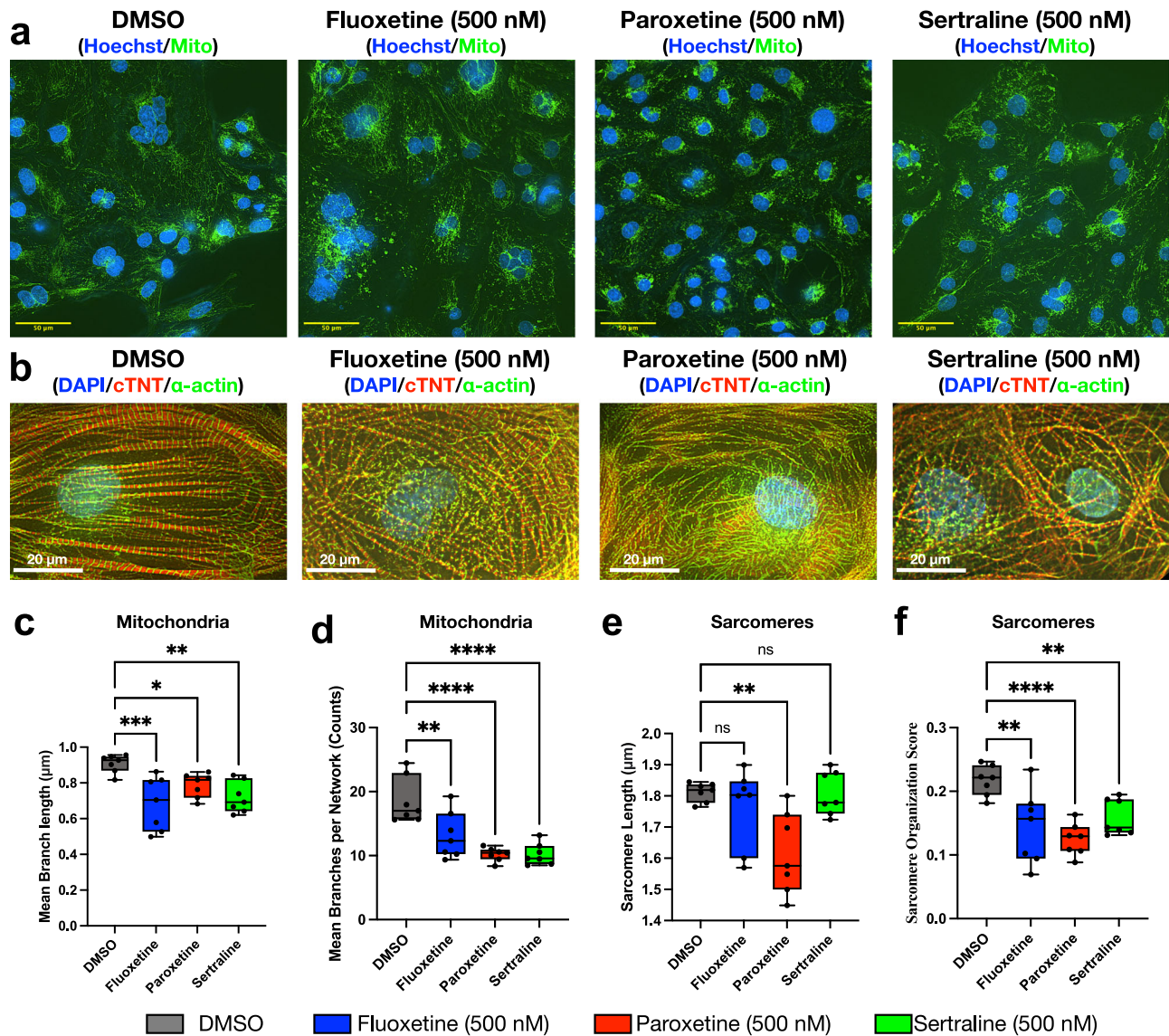


**Fig. 3 | Fluorescence staining of mitochondria and sarcomere of differentiating cardiomyocytes.** **a** Fluorescence staining of mitochondria in H1-CMs with Mito-Tracker (green for mitochondria and blue for cell nucleus). **b** Immunofluorescence staining of sarcomere with the primary antibodies of cTNT and  $\alpha$ -actinin in H1-CMs (green for  $\alpha$ -actinin, red for cTNT, and blue for cell nucleus). The mean branch length (**c**) and branches per network (**d**) of mitochondria were calculated by Fiji/

ImageJ with the MiNA plugin.  $n = 7$  biological replicates of each group for (**c** and **d**). Fast Fourier transformation (FFT) analysis showed the sarcomere length (**e**) and the sarcomere organization score (**f**) of  $\alpha$ -actinin signal distribution in the H1-CMs. \*indicates  $p < 0.05$ , \*\*indicates  $p < 0.01$ , \*\*\*indicates  $p < 0.001$ , \*\*\*\*indicates  $p < 0.0001$ , ns indicates no significance.  $n = 7$  biological replicates of each group for (**e** and **f**).

between the three groups, which may indicate the activation of different regulatory mechanisms (Fig. 4c, Supplementary Data 1). Several representative genes were displayed in the Volcano plot of DEGs (Fig. 4d–f). The relationship network of DEGs in each group associated with Gene Ontology biological process (GO-BP) terms was displayed to indicate which DEGs were caused by SSRIs that may lead to the dysregulation of ROS, ATP production and mitochondrial function (Fig. 4g–i). We also found that increased phosphoglycerate mutase 5 (*PGAM5*) expression was highly associated with the “regulation of mitochondrial fission” after paroxetine exposure, indicating that damaged mitochondria induced *PGAM5* to activate mitochondrial biogenesis and mitophagy to promote a cellular compensatory response (Figs. 3a, c, d, and 4h). The myosin heavy chain 7 (*MYH7*) showed a significant decrease and was highly associated with the “sarcomere organization” after three SSRIs exposure (Fig. 4g–i). Significant disarrangement in sarcomere structure was also observed due to SSRIs exposure (Fig. 3b, e, f), indicating that SSRIs may

cause disarrangement of the sarcomere structure by dysregulating *MYH7* expression. These results suggested that developmental exposure to SSRIs increased ROS levels, inhibited ATP production and mitochondrial respiration, and disrupted mitochondrial homeostasis and sarcomere structure in the differentiating H1-CMs, exerting high risks of dysfunction or abnormality of cardiomyocytes. To further explore the regulatory mechanisms underlying SSRIs-induced transcriptional changes in cardiomyocytes, we performed Gene Set Enrichment Analysis (GSEA) using the C3 collection from MSigDB, which includes transcription factor (TF) and microRNA (miRNA) target gene sets. Significant enrichment of some representative TF and miRNA targets was observed in response to fluoxetine, paroxetine, and sertraline exposure when compared to controls, suggesting that SSRIs may modulate specific regulatory networks involved in cardiac function and development (Supplementary Fig. 3). Thus, in the following experiments, we further applied a 3D-cardiac organoid model to investigate the toxicity effects of paroxetine on the cardiac system.

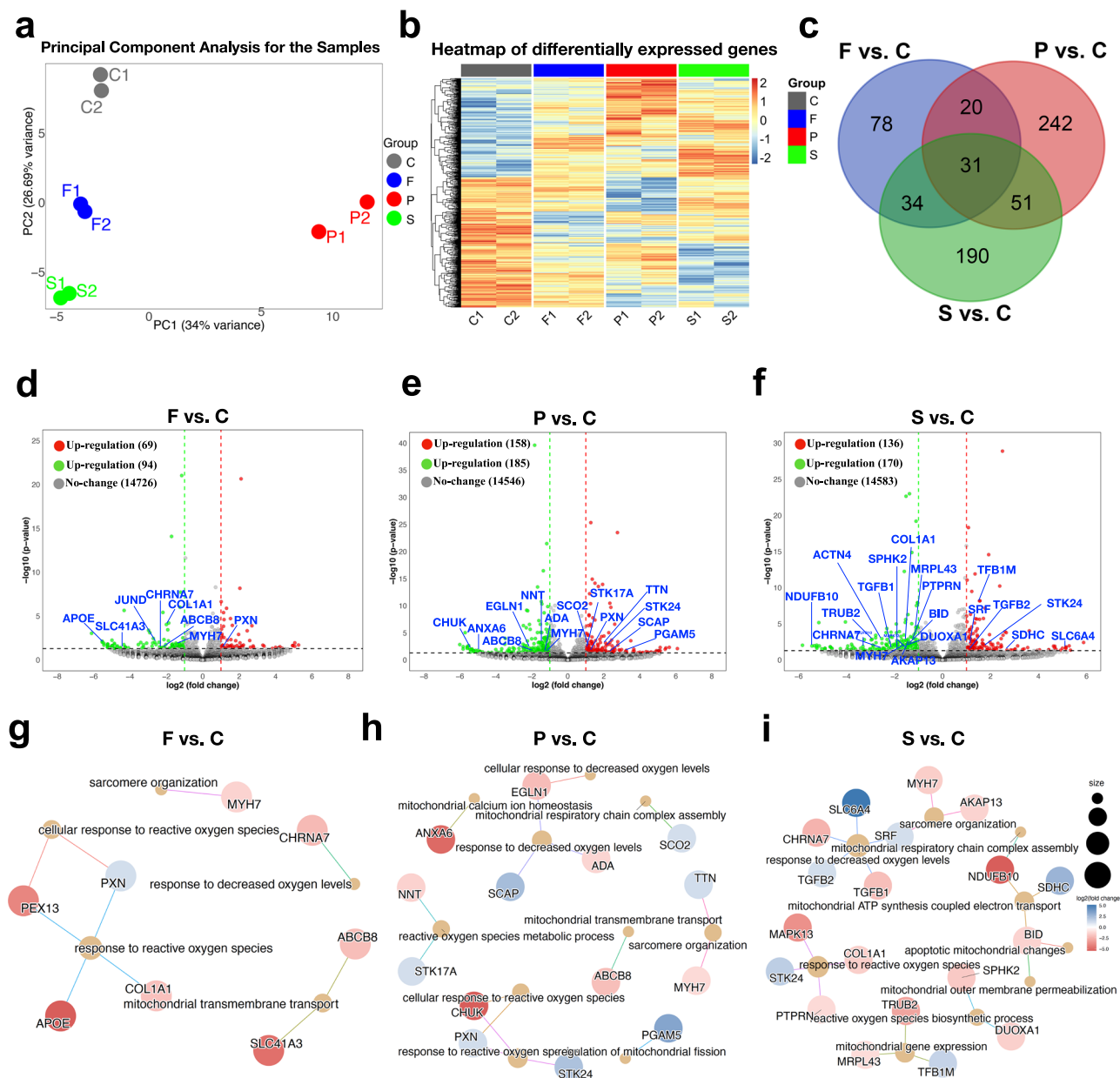


**Fig. 4 | Transcriptomic analysis of SSRIs toxicity in the 2D model. a** Principal component analysis for the samples. **b** Heatmap indicates the overall DEG expression pattern of all 4 groups of samples: C (control, DMSO), F (fluoxetine), P (paroxetine), and S (sertraline). **c** Comparison of the number of shared and distinct DEGs in three SSRIs compared to control. **d–f** Volcano plot showed the top altered genes after three SSRIs compared to control. Some representative genes are

highlighted in blue in the plot. **g–i** GO-BP terms and DEGs relationship network in three SSRIs compared to control. Each yellow node (circle) represents distinct GO-BP terms, and the circle size indicates the number of differentially expressed genes in the term. The edges represent categories of GO-BP terms with different color lines.

### SSRIs toxicity on developmental 3D-cardiac organoids

To further investigate the developmental toxicity of SSRIs on the cardiac system during differentiation, we employed a 3D cardiac organoid model and generated a simplified workflow schematic using BioRender (<https://www.biorender.com/>) (Fig. 5a). First, we identified the NOAEL of three SSRIs during the entire differentiation process and we determined 1000 nM as the NOAEL for all three SSRIs (Fig. 5b). Developmental exposure to SSRIs at 1000 nM did not cause obvious alterations in the size of the cardiac organoids, but organoids were found to be enlarged and non-beating at 2000 nM (Fig. 5c, Supplementary Fig. 4). However, long-term exposure to SSRIs at NOAEL impaired mitochondrial basal and maximal respiration, and decreased spare respiration capacity and ATP production (Fig. 5d–h). These results suggested that the 3D-cardiac organoid model can recapitulate the

toxicity outcomes as in the 2D model. The beating cardiac organoids exposed to SSRIs were attached in Supplementary Movies 1–4.

### Histology and immunofluorescence staining of 3D model

Histological analysis was performed from both control and paroxetine-treated 3D-cardiac organoids, which both showed the inner core (IC), the outer layer (OL), endodermal cavities (END CAV, which is in the IC), and the endodermal islands (END ISL, which is in the OL) (Supplementary Fig. 5). We further performed the immunofluorescence staining of the 3D model with antibodies of cluster of differentiation 31 (CD31), Wilms' tumor 1 (WT1), cardiac troponin T (cTNT), and  $\alpha$ -actinin (Fig. 6a). CD31 is a marker of endothelial cells and WT1 is essential for cardiac development. The results suggested that CD31 was increased and WT1 was decreased

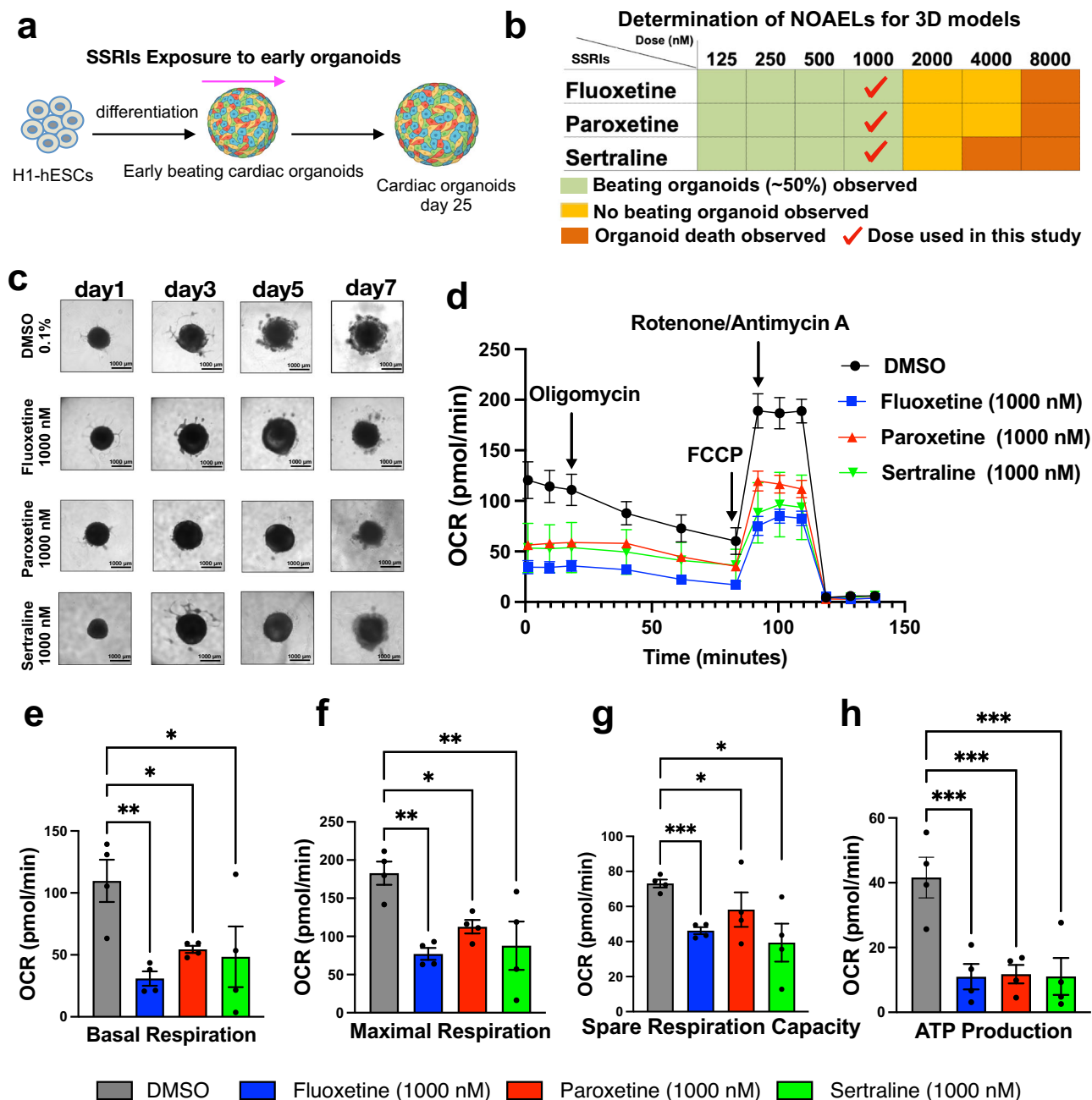


**Fig. 5 | SSRIs toxicity on differentiating cardiac organoids.** **a** The procedure of SSRIs treatment on differentiating cardiac organoids. **b** The identification of NOAEL of three SSRIs during the entire differentiation process of cardiac organoids. **c** The morphology changes of cardiac organoids derived from H1-hESCs. **d–h** The mitochondrial respiration levels of SSRIs toxicity on differentiating cardiac

organoids. **d** Graphical representation of the mitochondrial stress test. **e** Basal respiration, **f** maximal respiration, **g** spare respiration capacity, **h** ATP-linked respiration. \*indicates  $p < 0.05$ , \*\*indicates  $p < 0.01$ , \*\*\*indicates  $p < 0.001$ .  $n = 4$  biological replicates for all groups.

(Fig. 6b, c), which indicates SSRIs may impair cardiac development and promote angiogenesis. cTNT and  $\alpha$ -actinin showed no significant changes (Fig. 6d, e). These results also suggested the disparities of using 2D- and 3D-models for toxicology research. We can identify more comprehensive and sophisticated alterations in the 3D model than in the 2D model.

#### Transcriptome profiling revealed distinct biological processes related to SSRIs toxicity in the 3D model

The PCA and inter-sample correlation analysis revealed similar expression patterns and clustering in replicate samples (Fig. 7a). Based on the RNA-seq analysis from 3D-cardiac organoids upon developmental exposure to paroxetine, the expression profiles of DEGs were extracted and displayed by

clustering heatmaps, showing significant differences in the comparison groups (Fig. 7b). We identified 919 DEGs in the paroxetine-treated organoids compared to the control group, with some representative genes highlighted in blue in the plot (Fig. 7c, Supplementary Data 2). The significantly up-regulated genes fibrinogen beta chain (*FGB*) and vitronectin (*VTN*) were associated with “regulation of hemostasis”, “negative regulation of blood coagulation”, and “regulation of mitochondrion organization”. On the other hand, the down-regulated genes ankyrin repeat domain 1 (*ANKRD1*) and *MYH7* were associated with “sarcomere organization” and “cardiac muscle tissue morphogenesis”, myosin light chain-2 (*MYL2*) was associated with “cardiac muscle tissue morphogenesis”, cytochrome P450 2J2 (*CYP2J2*) was associated with “xenobiotic metabolic process”,



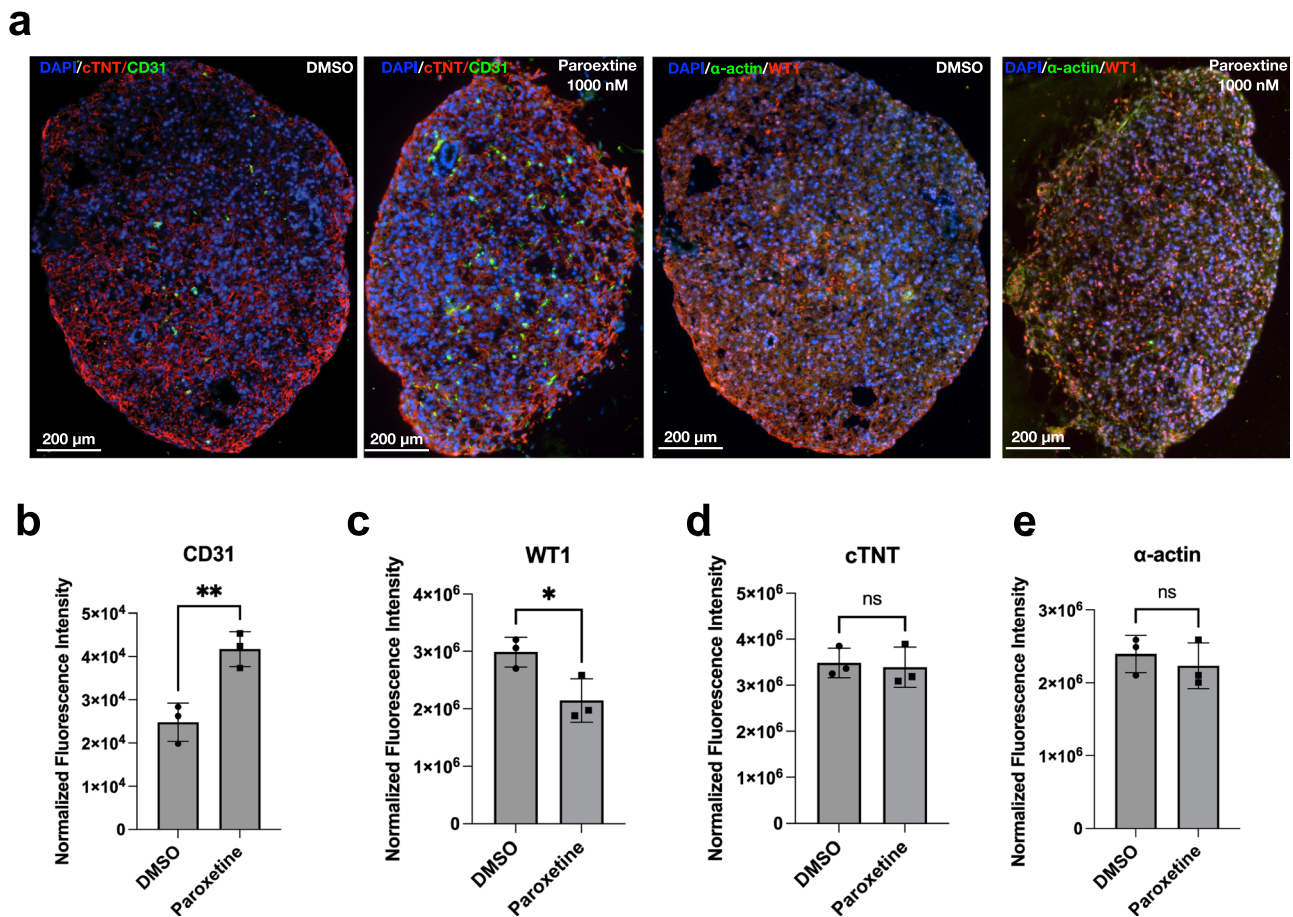


**Fig. 6 | Immunofluorescence staining of 3D model.** **a** Immunofluorescence staining of sarcomere with the primary antibodies of CD31, WT1, cTNT, and α-actinin in 3D-model. **b–e** The fluorescence intensity was calculated by Fiji/ImageJ

and normalized to cell counts. **b** CD31, **c** cTNT, **d** WT1, **e** α-actinin. \* indicates  $p < 0.05$ . ns indicates no significance.  $n = 3$  biological replicates for all groups.

and immediate early response 3 (*IER3*) was associated with “regulation of mitochondrial organization” (Fig. 7d–f). In particular, the expression of *MYH7* was significantly decreased after 3D-cardiac organoids were exposed to paroxetine, which is consistent with the results in 2D-monolayer cardiomyocytes (Figs. 7f and 4h). Besides, we noticed that the 9 genes, including titin-cap (*TCAP*), *MYH7*, *ANKRD1*, myozenin 1 (*MYOZ1*), limonin 2 (*LMOD2*), troponin T1 (*TNNT1*), synaptopodin 2 like (*SYNP2L*), cysteine and glycine rich protein 3 (*CSRP3*), and calsequestrin 1 (*CASQ1*), related to the sarcomere organization were all decreased except for bone morphogenetic protein 10 (*BMP10*) (Fig. 7f), which implied that the sarcomeric structure disarrangement. We validated the expression of these representative genes by real-time quantitative PCR (qPCR), which was highly consistent with the RNA-seq results (Fig. 7g), underscoring the reliability and accuracy of our RNA-seq data. We further investigated the regulatory mechanisms underlying SSRI-induced transcriptional changes in 3D cardiac organoids by performing GSEA using C3 gene sets, which include TF and miRNA target gene sets. Notably, significant enrichment of some representative TF and miRNA targets was observed in response to paroxetine compared to controls, offering valuable insights for future studies on regulatory pathways, particularly integrated with GSEA analyses of 2D cardiomyocyte models (Supplementary Fig. 6).

## Discussion

SSRIs have been found to be toxic to the cardiovascular system in both adult and early developmental stages during pregnancy<sup>8</sup>. Previous animal studies suggested that serotonin and its receptors play a critical role during heart development and cardiomyocyte function by regulating mitochondrial function. Serotonin has been reported to possess significant effects on

cardiac activities and is a novel survival factor targeting mitochondria in cardiomyocytes<sup>22</sup>. Serotonin can directly activate its functional receptors on the mitochondrial membrane, and regulate mitochondrial and cellular activities and functions<sup>23</sup>. Serotonin can also be a regulator of mitochondrial biogenesis and function in rodent cortical neurons, via a 5-HT2A receptor-mediated recruitment of the SIRT1–PGC-1α axis<sup>24</sup>. However, continuous SSRIs treatment causes an adaptive fall in 5-HT metabolism and synthesis<sup>25</sup>, suggesting that SSRIs may cause cardiac toxicity via dysfunction of mitochondria. It is crucial to unravel the intricate effects of SSRIs on both cardiac and mitochondrial function, particularly considering their potential adverse effects during the critical phase of early human heart development.

The clinical study estimated that the median drug concentrations in umbilical cord serum of fluoxetine, paroxetine, and sertraline to be 6.0–201.0 ng/ml, 3.0–31.0 ng/ml, and 1.0–35.0 ng/ml, respectively<sup>21</sup>. The fetal exposure levels vary among SSRI drugs measured in the umbilical cord and show significant inter-individual variabilities<sup>26</sup>. Our results showed that intracellular ROS levels were significantly increased, and ATP production and mitochondrial respiration were decreased in the differentiated cardiomyocytes after exposure to SSRIs. These results suggested that long-term exposure to clinical levels of SSRIs induced mitochondrial dysfunction, ultimately decreasing ATP production. During the first trimester of pregnancy, exposure to paroxetine, fluoxetine, and sertraline have demonstrated an approximate increased likelihood of congenital heart defects by 1.6, 1.4, and 1.3 times, respectively<sup>13</sup>. In particular, paroxetine use during the first trimester of pregnancy is highly associated with an increased risk of major congenital malformations and cardiac malformations<sup>27–29</sup>. During our development exposure experiment of 2D and 3D models, ATP production

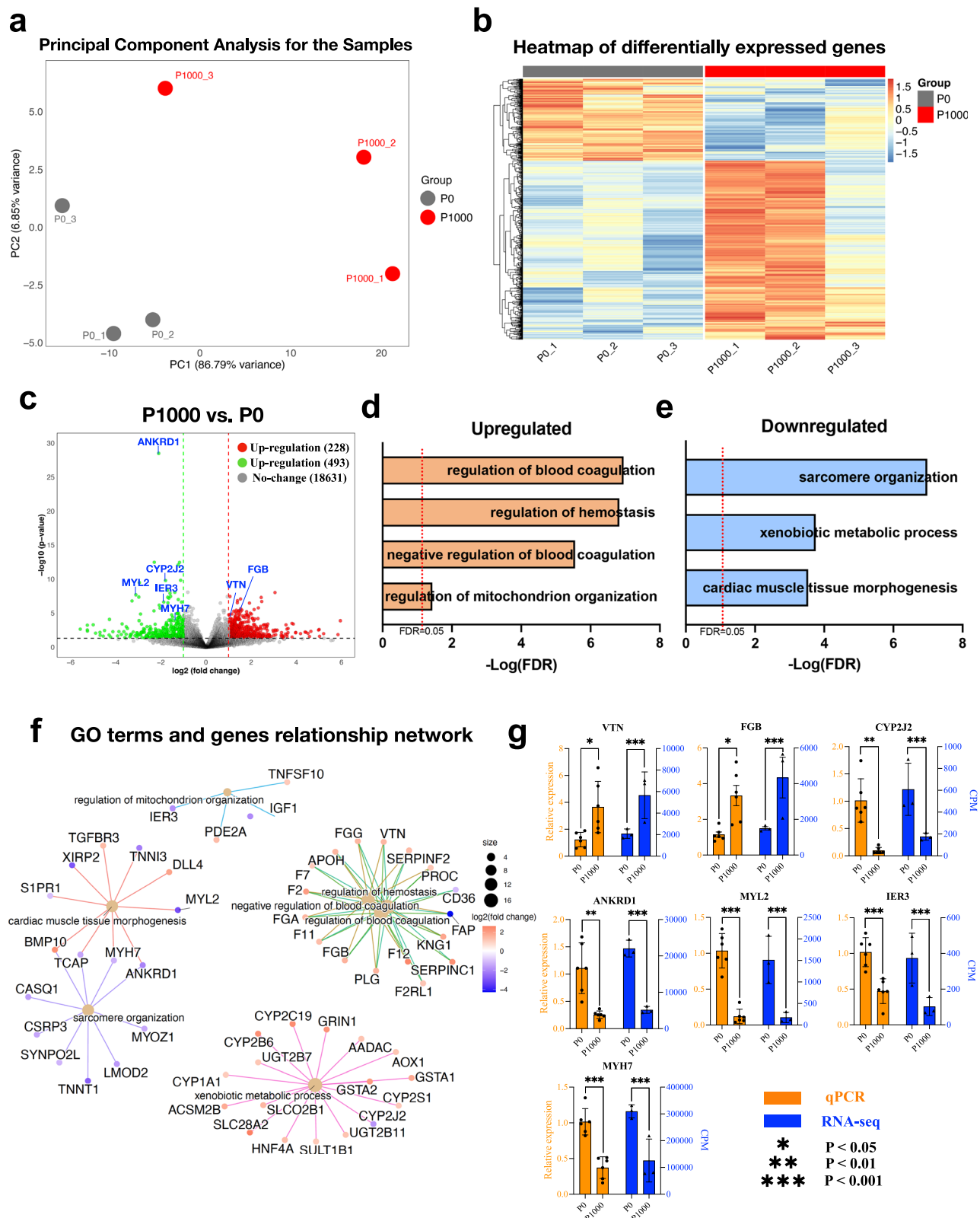


**Fig. 7 | Transcriptomic analysis of SSRIs toxicity in the 3D model. a** Principal component analysis for the samples. **b** Heatmap indicates the overall DEG expression pattern of 2 groups of samples: P1000 (paroxetine, 1000 nM) and P0 (paroxetine, 0 nM). **c** Volcano plot showed the DEGs between paroxetine and control. Some representative genes are highlighted in blue in the plot. **d, e** GO-BP terms enrichment in paroxetine compared to control. **f** GO-BP terms and DEGs

relationship network in paroxetine compared to control. Each yellow node (circle) represents distinct GO-BP terms, and the circle size indicates the number of differentially expressed genes in the term. The edges represent categories of GO-BP terms with different color lines. **g** The identification of RNA-seq was verified by qPCR. \* indicates  $p < 0.05$ , \*\* indicates  $p < 0.01$ , \*\*\* indicates  $p < 0.001$ . For qPCR,  $n = 6$  biological replicates; for RNA-seq,  $n = 3$ .



and mitochondrial respiration were impaired upon exposure to NOAEL of SSRIs, indicating that SSRIs toxicity on cardiac development.

Mitochondria play key roles in cardiac development and homeostasis, and mitochondrial damage is highly associated with mitochondrial cardiomyopathy, congenital heart disease, coronary heart disease, myocardial ischemia-reperfusion injury, heart failure, and drug-induced cardiotoxicity<sup>30</sup>. Mitochondria are not only a source of ATP energy but also generators of ROS, that cause oxidative damage<sup>31</sup>. Excess ROS production and oxidative damage are associated with cardiac pathology. Antioxidant defenses, mitochondrial quality control, mtDNA maintenance mechanisms as well as mitochondrial fusion and fission improve mitochondrial function and cardiomyocyte survival under stress conditions<sup>32</sup>. The structural specialization includes the expansion of the mitochondrial network by fission and fusion of mitochondria, which is not restricted to cardiomyocyte development but also later on required for the maintenance of a healthy heart<sup>32</sup>. In our study, developmental exposure to SSRIs resulted in smaller mitochondria branch sizes compared and fewer branches per network indicating that mitochondrial homeostasis of cardiomyocytes was impaired. We also noticed that the *PGAM5* gene significantly increased after paroxetine treatment. *PGAM5* was identified as a crucial regulator in maintaining mitochondrial homeostasis<sup>33</sup>. *PGAM5* activates mitochondrial biogenesis and mitophagy to promote a cellular compensatory response when mitochondria are mildly damaged, whereas severe damage to mitochondria leads to *PGAM5*-induced mitochondria fission, disruption to mitochondrial movement, and amplification of apoptosis, necroptosis and mitophagy death signals, which eventually evoke cell death<sup>34</sup>. Moreover, *PGAM5* plays a key role in oxidative stress-induced necroptosis, which increases the level of Cyclophilin D phosphorylation to open mitochondrial permeability transition pores and increase ROS production in cardiac ischemia-reperfusion injury<sup>35</sup>. Our result also showed similar results that cardiomyocyte ROS increased after SSRIs exposure. Consequently, there was a notable increase in ROS, a decline in ATP production, and mitochondrial respiration that may be caused by *PGAM5* activating mitochondrial excessive fission after exposure to SSRIs.

From the 2D- and 3D-models used in this study, we also found that the genes related to sarcomere organization of GO-BP terms were dysregulated, and the sarcomere structure exhibited disarrangement. Sarcomere is the basic contracting unit in cardiac muscles. Genetic mutation in genes coding sarcomeric proteins can cause impairments in the structure integrity and function of the sarcomere<sup>36,37</sup>. In the heart, mutations in sarcomeric proteins are responsible for the majority of genetically inherited cardiomyopathies<sup>36</sup>. *MYH7*, a sarcomeric gene encoding the myosin heavy chain, which mutations affect the structure and physiologic function of sarcomere, thus resulting in cardiomyopathy<sup>37</sup>. The two major types of *MYH7*-related inherited cardiomyopathy include hypertrophic cardiomyopathy and dilated cardiomyopathy. Restricted cardiomyopathy, left ventricular non-compaction cardiomyopathy, congenital heart defects, arrhythmia, etc., can be affected as well<sup>37</sup>. *MYH7* showed a significant decrease both in 2D-monolayer cardiomyocytes and 3D cardiac organoids after SSRIs exposure. Significant disarrangement in sarcomere structure was also observed in response to paroxetine exposure, indicating that SSRIs may cause disarrangement of the sarcomere structure by dysregulating *MYH7* expression.

From the immunofluorescence staining results of 3D-cardiac organoids, we noticed that the CD31 signal increased after paroxetine exposure. CD31 is a reliable marker for identifying endothelial cells<sup>38</sup>. The up-regulated CD31 indicates endothelial cells increasing, which means angiogenesis may be promoted after paroxetine exposure. It has been reported that hippocampal angiogenesis is increased with SSRIs use in major depression<sup>39</sup>. Fluoxetine improves the angiogenic parameters and restores neovascularization in animals exposed to psychological stress<sup>40</sup>. SSRIs may induce changes in TGF $\beta$  signaling, leading to a change in placental angiogenesis and barrier formation<sup>41</sup>. Moreover, we found that WT1 decreased after paroxetine exposure. WT1 is essential and required for many aspects of cardiac development. WT1 is associated with key processes such as the formation of the epicardium, valves, and myocardial wall maturation<sup>42</sup>.

Ablation of WT1 leads to abnormal development of the sinus venosus and atrium, absence of pectinate muscles, and a thin ventricular myocardium<sup>43</sup>. While there is a dearth of relevant studies on the effects of SSRIs on cardiac development and angiogenesis in the heart, our findings indicate potential roles for SSRIs in impairing cardiac development and promoting angiogenesis. Nonetheless, it is imperative to underscore the necessity for additional evidence and comprehensive investigations to corroborate these preliminary observations.

Based on the RNA-seq analysis from 3D-cardiac organoids upon developmental exposure to paroxetine, the significantly up-regulated genes *FGB* and *VTN* were related to the regulation of hemostasis and negative regulation of blood coagulation. It has also been reported that SSRIs treatment is associated with abnormal bleeding and coagulation disorder because these drugs can directly influence 5-HT, which is involved in platelet aggregation and hemostasis<sup>44,45</sup>. *IER3* is involved in preventing the production of ROS in mitochondria, and consequently, null mutation of *IER3* increases the production of mitochondrial ROS<sup>46</sup>. Our result showed that *IER3* was significantly reduced and involved in the regulation of mitochondrial organization, suggesting that increased mitochondrial ROS leads to decreased mitochondrial respiration. *ANKRD1* is a sarcomere-localized transcriptional cofactor, and mutations in *ANKRD1* have been shown to be associated with hypertrophic and dilated cardiomyopathy<sup>47</sup>. Our results also indicated that *ANKRD1*, same as *MYH7*, was significantly reduced and involved in the regulation of sarcomere organization, further providing evidence for the consequences of sarcomeric structure disarrangement. Furthermore, our results showed that the 9 genes (*TCAP*, *MYH7*, *ANKRD1*, *MYOZ1*, *LMOD2*, *TNNT1*, *SYNPO2L*, *CSRP3*, *CASQ1*) related to the sarcomere organization were all decreased except for *BMP10*, which explained the sarcomeric structure disarrangement. *MYL2* is also a sarcomeric protein and a member of the EF-hand calcium-binding protein family, which is involved in heart muscle structure and function<sup>48</sup>. Our result showed that *MYL2* was significantly decreased and involved in cardiac muscle tissue morphogenesis, implying that disorder of cardiac muscle structure and function after SSRIs exposure.

In conclusion, our study demonstrated that SSRIs induced cardiac toxicity via dysfunction of mitochondria and sarcomere structure, as observed at both morphological and phenotypic levels on 2D-monolayer cardiomyocytes and 3D-cardiac organoids. We also elucidated mechanisms of SSRIs-induced dysfunction in mitochondria and sarcomere structure through transcriptomic analysis of 2D and 3D models, underscoring that *PGAM5* and *MYH7* may have important roles in these processes. Furthermore, our data suggested that SSRIs may be associated with abnormal bleeding and coagulation disorder, as well as impair cardiac development and promote angiogenesis from the 3D model analysis. These findings highlight the potential risks of SSRIs to cardiac health and contribute to a deeper understanding of their side effects and mechanisms. It may also inform future strategies for safer antidepressant therapies.

## Methods

### Chemicals

Fluoxetine (cat. no. F07501G), paroxetine (cat. no. 50-612-50001), and sertraline (cat. no. AC462190010) were purchased from Fisher Scientific and then dissolved in DMSO (cat. no. D2650, Sigma-Aldrich) as stocks. Afterwards, they were diluted to the final working concentration in the medium for experiments.

### Stem cell lines and cell culture

The H1-hESCs used in this study were obtained from WiCell (Wisconsin, USA). The hiPSCs were used in this study obtained from the Stanford Cardiovascular Institute (SCVI) Biobank, Stanford University. It was generated through reprogramming of peripheral blood mononuclear cells from an anonymous healthy individual with the Sendai virus. Stem cells were grown in Matrigel, hESC-qualified (cat. no. 354277, Corning)-coated 12-well plates in Essential 8™ Medium (E8 medium) (cat. no. A1517001, Thermo Fisher Scientific) at 37 °C in 5% CO<sub>2</sub> in compressed air and high

humidity. This study involved the use of H1-hESCs and hiPSCs reprogrammed from peripheral blood mononuclear cells and was approved by the Clemson University Human Subjects Research Institutional Review Board. All ethical regulations relevant to human research participants were followed.

## 2D-monolayer cardiomyocytes exposed to SSRIs

For 2D-monolayer cardiomyocyte differentiation, a well-established protocol was used to generate beating cardiomyocytes derived from H1-hESCs or hiPSCs<sup>49</sup>. Beating cardiomyocytes will generally appear in about 8 days, and the cells can be further treated with glucose-free RPMI/1640 medium (cat. no. 11879020, Gibco) with B27 supplement (cat. no. 17504044, Thermo Fisher Scientific) for 2 rounds. For differentiated cardiomyocytes derived from both H1-hESCs (i.e., H1-CMs) and hiPSCs (i.e., hiPS-CMs), H1-CMs and hiPS-CMs were exposed to three clinical levels of SSRIs i.e., 30 nM (sertraline), 55 nM (paroxetine), and 263 nM (fluoxetine) for five days at day 30 which were used to analyze the clinical levels of SSRIs toxicity<sup>21</sup>. For developmental exposure, the SSRIs were added into the medium when we replaced the culture medium following the differentiation protocol. After obtaining beating H1-CMs, the medium with drugs was replaced every two days until day 25. We evaluated NOAEL of SSRIs on differentiating cardiomyocytes using the graded concentration with 125 nM, 250 nM, 500 nM, 1000 nM, 2000 nM, and 4000 nM. Cardiomyocytes treated with 0.1% DMSO were used as the control group.

## Cell culture and cardiac organoids differentiation exposed to SSRIs

For 3D-organoid differentiation, a scaffold-free 3D-cardiac organoid method was used<sup>17</sup>. Briefly, 5000 H1-hESCs were seeded into a 96-well Clear Round Bottom Ultra-Low Attachment Microplate (cat. no. 7007, Corning) with 100 µl E8 medium containing 10 µM Y-27632 ROCK Inhibitor (cat. no. 7000, Tocris), and then the plate was centrifuged at 1600 rpm for 5 min. After 2 days, the 3D spheroids can be observed and then were removed and embedded into a 20 µl Matrigel Membrane Matrix (cat. no. 356234, Corning) in a new ultra-low-attachment 96-well round bottom plate, using a blunt 10 µl tip. After embedding, the plate was placed in the 37 °C incubator for 1 h to solidify the Matrigel droplet, then add 200 µl of E8 medium. After 2 days (day 0), cardiac differentiation was initiated by replacing the medium with RPMI/1640 medium (cat. no. 11875093, Gibco) with B27 supplement without insulin (cat. no. A1895601, Thermo Fisher Scientific) and 7.5 µM CHIR99021 (cat. no. 4423, Tocris). After 24 h (day 1), the medium was replaced with RPMI/1640 medium with B27-insulin. On day 3, the medium was replaced with RPMI/1640 medium with B27-insulin and 5 µM IWP2 (cat. no. 3533, Tocris). On day 5, the medium was replaced with RPMI/1640 medium with B27 supplement without insulin. The beating cardiac organoids can be observed around day 9, then the medium was replaced with RPMI/1640 medium with B27 containing insulin. On day 12, 60 µl Cell Recovery Solution (cat. no. CB-40253, Corning) was added to dissolve the Matrigel by putting the plate at 4 °C for 20 min. After that, the organoids were removed to a low-attachment 24-well plate using a blunt 1000 µl tip. The cardiac organoids were then cultured until day 25, and changed the RPMI/1640 medium with B27 containing insulin every two days. During this procedure, SSRIs with final concentrations of 1000 nM were added at each step of medium replacement after obtaining beating cardiac organoids.

## Microscopy and high-content imaging

The microscopy of the 3D spheroids was conducted using a Nikon motorized Ti2E microscope with a stage-top incubator (In Vivo Scientific, SC, USA). Reactive oxygen species (ROS), ATP production, mitochondrial membrane potential, and mean mitochondrial branch size and network of cardiomyocytes were evaluated using an imaging-based multi-parametric analysis strategy (i.e., high content imaging). Cardiomyocytes were re-plated into optical 96-well plates, and cells were labeled with the following fluorescent dyes: Fluorometric Intracellular ROS Kit (cat. no. MAK143,

Sigma-Aldrich) for ROS assay, BioTracker ATP-red live cell dye (cat. no. SCT045, Sigma-Aldrich) for ATP production assay, and MitoProbe™ TMRM Assay Kit (cat. no. M20036, Thermo Fisher Scientific) for mitochondrial membrane potential assay. The fluorescence intensities were quantified using a Cytation 5 Cell Imaging Multimode Reader with Gen5 Image Prime software (Biotek, Winooski, VT, USA). For mitochondrial morphology analysis, 200 nM of MitoTracker Green FM (cat. no. M46750, Thermo Fisher Scientific) was used for staining live mitochondria. The cell nucleus was stained by Hoechst (cat. no. 14533, Sigma-Aldrich). The images were taken using a Nikon Ti2-E fluorescence microscope, and then mitochondrial morphology was analyzed using the Fiji/ImageJ software with MiNA plugin<sup>50</sup>.

## Immunofluorescence staining of sarcomere in cardiomyocytes

The cardiomyocytes were re-plated in Nunc™Lab-Tek™II glass-bottomed 8-chamber glass slides (cat. no. 177402, Thermo Fisher Scientific), and then cells were fixed and permeated in the plate using a Human Cardiomyocyte Immunocytochemistry Kit (cat. no. A25973, Thermo Fisher Scientific). The primary antibodies included rabbit anti-cTNT (cat. no. ab45932, 1:500, Abcam) and mouse anti-α-actinin (sarcomeric) (cat. no. ab9465, 1:500, Abcam). The secondary antibodies included goat anti-rabbit IgG, Alexa Fluor 594 (cat. no. R37117, 1:500, Thermo Fisher Scientific) and goat anti-mouse IgG, Alexa Fluor 488 (cat. no. A-11001, 1:500, Thermo Fisher Scientific). The cell nuclear was stained by DAPI (cat. no. D9542, Sigma-Aldrich). The images were taken using a Nikon Ti2-E fluorescence microscope with a 60X oil-immersed objective. For subsequent data analysis, to measure the sarcomeric disarrangement in paroxetine-treated cells, we analyzed the immunofluorescence staining images. Sarcomere arrangement signals were extracted from each image and subjected to in-depth analysis, including sarcomere length and sarcomere organization score, through Fast Fourier Transformation (FFT) method with SotaTool software<sup>51</sup>.

## Histology analysis and immunofluorescence staining of 3D-cardiac organoids

The cardiac organoids were fixed in 4% paraformaldehyde (cat. no. 100496, Sigma-Aldrich), further dehydrated through a graded ethanol (cat. no. BP28184, Fisher Scientific) series (70%, 80%, 90%, and 100%), transparentized in xylene (cat. no. 534056, Sigma-Aldrich), and finally embedded in paraffin blocks. The paraffin blocks were cut into 8 µm thick sections by using a Semi-Automated Rotary Microtome (Leica, Wetzlar, Germany) and stained with hematoxylin and eosin (H&E) by H&E staining kit (cat. no. ab245880, Abcam) following standard procedures of H&E Staining System (Leica). Microscopic examination was observed using a Nikon Y-TV55 microscope and photographed with a Nikon DS-Ri2 (Nikon). For IF staining, the cardiac organoid paraffin sections were immersed in xylene 2 times for 10 min each, then rehydrated through a graded ethanol series (100%, 90%, 80% and 70%) for 5 min each. Rinse the sections with deionized H<sub>2</sub>O then followed by antigen retrieval using Antigen Retrieval Reagent, pH 9 (cat. no. ENZACC1130100, Enzo Life Sciences). Block non-specific staining between the primary antibodies and the cardiac organoid by incubating in blocking buffer (5% BSA in PBS, cat. no. AAJ61089AK, Thermo Fisher Scientific) for 30 min at room temperature. Incubate the sections overnight at 4 °C in the primary antibodies, including rabbit anti-cTNT (cat. no. ab45932, 1:500, Abcam), rabbit anti-WT1 (cat. no. ab89901, 1:200, Abcam), mouse anti-α-actinin (cat. no. ab9465, 1:500, Abcam), and mouse anti-CD31 (cat. no. ab9498, 1:200, Abcam). Incubate the sections for one hour at room temperature in the secondary antibodies, including goat anti-rabbit IgG, Alexa Fluor 594 (cat. no. R37117, 1:500, Thermo Fisher Scientific) and goat anti-mouse IgG, Alexa Fluor 488 (cat. no. A-11001, 1:500, Thermo Fisher Scientific). The cell nucleus was stained by DAPI for 15 min. Sections were mounted with Anti-Fade Fluorescence Mounting Medium (cat. no. ab104135, Abcam). The images were taken using a Nikon Ti2-E fluorescence microscope with a 10X objective.

## Mitochondrial respiratory activity assay

For the 2D-monolayer cardiomyocytes, the mitochondrial respiratory activity in cardiomyocytes was analyzed by mitochondrial stress test using a Seahorse XFe24 Extracellular Flux Analyzer (Agilent, Santa Clara, CA, USA). 50,000 cells were plated into an XFe24 cell culture microplate (Agilent) with RPMI/1640 and B27 supplemented with 10% FBS and 10  $\mu$ M ROCK inhibitor. After 48 h of recovery, the mitochondrial stress test was performed using a Seahorse XF Cell Mito Stress Test kit (including pyruvate, glutamine, and glucose) (cat. no. 103681-100, Agilent) according to the manufacturer's manual. Briefly, one day prior to the experiment, the XFe24 sensor cartridges were hydrated in XF calibrator solution (cat. no. 100840-000, Agilent) and incubated overnight at 37 °C in a non-CO<sub>2</sub> incubator. One hour prior to the experiment, the cells were incubated at 37 °C (non-CO<sub>2</sub>) in 500  $\mu$ l of Seahorse assay medium, containing XF base medium (cat. no. 103334-100, Agilent) supplemented with 1 mM pyruvate, 2 mM glutamine, and 10 mM glucose (pH 7.4). Mitochondrial respiratory activity was measured with sequential injections of 2  $\mu$ M oligomycin (cat. no. 75351, Sigma-Aldrich), 2  $\mu$ M carbonyl cyanide 4-(trifluoromethoxy) phenylhydrazone (FCCP) (cat. no. c2920, Sigma-Aldrich) and each 0.5  $\mu$ M of rotenone/antimycin A (cat. no. R8875 and A8674, Sigma-Aldrich). Data were normalized by cell-number counting using a TC20 automated cell counter (Bio-Rad, Hercules, CA, USA).

For the 3D-cardiac organoids, the mitochondrial respiratory activity in cardiac organoids was analyzed by mitochondrial stress test using a Seahorse XF Pro Analyzer (Agilent). Briefly, one day prior to the experiment, the XF Pro sensor cartridges were hydrated in XF calibrator solution and incubated overnight at 37 °C in a non-CO<sub>2</sub> incubator. One hour prior to the experiment, the cardiac organoids were transferred to the Poly-D Lysine 100  $\mu$ g/mL coated Agilent Seahorse XFe96 Spheroid Microplates and incubated at 37 °C (non-CO<sub>2</sub>) in 175  $\mu$ l of Seahorse assay medium. Mitochondrial respiratory activity was measured with sequential injections of 5  $\mu$ M oligomycin, 2  $\mu$ M FCCP and each 2  $\mu$ M of rotenone/antimycin A. Data were normalized by the total amount of DNA of each cardiac organoid extracted using DNeasy Blood & Tissue Kit (cat. no. 69504, Qiagen).

## RNA-sequencing and data analysis

Total RNA was extracted using the miRNeasy Mini Kit (cat. no. 217084, Qiagen), and RNA was then subjected to RNase-Free DNase (cat. no. 79254, Qiagen) digestion and purified using the RNeasy Kits for RNA Purification (cat. no. 74104, Qiagen) according to the manufacturer's instructions. RNA integrity was checked with Cytation 5, and only samples with a 260/280 ratio of around 2.0 were used for RNA-sequencing preparation. cDNA Libraries were prepared following the DNBSEQ Eukaryotic Stranded Transcriptome library preparation pipeline. mRNA was enriched with Oligo dT selection and fragmentation. First-strand cDNA was synthesized using random N6-primed reverse transcription and dUTP for second-strand synthesis. Ends were repaired, 3' adenylated, and adapters ligated. cDNA was amplified by PCR, denatured by heat, and cyclized by splint oligo and DNA ligase. Sequencing of the cDNA libraries was done on the DNBSEQ platform. Sequencing reads were inspected by FastQC (v0.12.1, <http://www.bioinformatics.babraham.ac.uk/projects/fastqc/>) and trimmed through Trim Galore (v0.6.7, [https://www.bioinformatics.babraham.ac.uk/projects/trim\\_galore/](https://www.bioinformatics.babraham.ac.uk/projects/trim_galore/)) to retain high-quality clean reads for subsequent analysis. All clean reads were appropriately mapped to the human reference genome (GRCh38) by using HISAT2 (v2.2.1)<sup>52</sup>. The gene expression quantification was carried out using HTSeq (v2.0.4)<sup>53</sup>, followed by the DESeq2 (v1.42.0)<sup>54</sup> package to obtain DEGs with the criteria of  $|\log_2(\text{fold change})| > 1$  and  $p\text{-value} < 0.05$ . GO-BP terms enrichment analysis was performed based on the DEGs between SSRIs-treated and control groups to identify functional attributes via clusterProfiler (v4.10.0)<sup>55</sup>. We prioritized GO-BP terms associated with mitochondrial and sarcomeric functions from the enriched results based on their relevance to the observed cellular phenotypes. GSEA was performed to identify enriched regulatory pathways in transcriptomic profiles of

cardiomyocytes treated with SSRIs. The resulting ranked gene lists were used for GSEA using the MSigDB C3 collection, which includes gene sets representing transcription factor targets (C3:TFT) and microRNA targets (C3:MIR). Enrichment was assessed using the clusterProfiler. Gene sets with a  $p\text{-value} < 0.05$  were considered significantly enriched. Enrichment results were visualized using bubble plots, indicating the gene ratio,  $p\text{-value}$ , and gene count per term, separated into activated and suppressed categories. For 2D-model RNA-seq, we set two replicates for each group. For 3D-model RNA-seq, we set three replicates for each group.

## RNA isolation and real-time quantitative PCR

Total RNA was extracted from organoids in each group using the miRNeasy Mini Kit according to the manufacturer's instructions. RNA integrity was checked with a Take3 microvolume plate in Cytation 5, and only samples with a ratio of 260/280 around 2.0 were subsequently used for qPCR. cDNA was synthesized from 500 ng of total RNA using iScript™ cDNA synthesis kits (cat. no. 1708890, BioRad) following the manufacturer's protocol. qPCR was performed with BioRad CFX Real-Time PCR System in 20  $\mu$ l reactions using 1  $\mu$ l of cDNA, 0.25  $\mu$ M of each forward and reverse primer and 1X iTaq™ Universal SYBR® Green Supermix (cat. no. 1725121, Bio-Rad). The qPCR program consisted of 1 cycle of 95 °C for 5 min; and 40 cycles of 95 °C for 15 s, 60 °C 30 s and 72 °C for 30 s. Primers used were ordered from Qiagen to amplify the genes, including *FGB*, *VTN*, *ANKRD1*, *MYL2*, *MYH7*, *CYP2J2*, and *IER3*. The 18S was used as a normalizing gene. A standard curve was generated to assess accuracy, and primers with an amplification efficiency of more than 95% were chosen for qPCR. Six biological and three technical replicates were used for each gene. The primers used in this study were displayed in Supplementary Table 1.

## Statistics and reproducibility

We conducted the statistical analysis using GraphPad Prism 10.2.1 (GraphPad Software, Inc., San Diego, CA). Nonparametric t-test was used to compare data between two groups and one-way ANOVA followed by Fisher's LSD test was used to compare data of multiple groups wherever appropriate. Data are presented as means  $\pm$  standard error of the mean (SEM). At least 3 biological replicates were used in each experiment. The number of biological replicates ( $n$ ) is detailed in the figure legends. For Bulk RNA sequencing data, statistical analyses were described as above.

## Reporting summary

Further information on research design is available in the Nature Portfolio Reporting Summary linked to this article.

## Data availability

The RNA-seq data generated for this work have been deposited in the NIH BioProject database (<https://www.ncbi.nlm.nih.gov/bioproject/>), and BioProject IDs are PRJNA1045682 for 2D-monolayer cardiomyocytes and PRJNA1045285 for 3D-cardiac organoids. The source data for the main and Supplementary Figs. are available as Supplementary Data 3, and all other data are available from the corresponding author on reasonable request.

Received: 6 June 2024; Accepted: 2 May 2025;

Published online: 12 May 2025

## References

- Xue, W. et al. Identification of the inhibitory mechanism of FDA approved selective serotonin reuptake inhibitors: an insight from molecular dynamics simulation study. *Phys. Chem. Chem. Phys.* **18**, 3260–3271 (2016).
- Feighner, J. P. Mechanism of action of antidepressant medications. *J. Clin. Psychiatry* **60**, 4–13 (1999).
- Cowen, P. J. Serotonin and depression: pathophysiological mechanism or marketing myth?. *Trends Pharmacol. Sci.* **29**, 433–436 (2008).



4. Lebin, L. G. & Novick, A. M. Selective serotonin reuptake inhibitors (SSRIs) in pregnancy: an updated review on risks to mother, fetus, and child. *Curr. Psychiatry Rep.* **24**, 687–695 (2022).
5. Molenaar, N. M. et al. The international prevalence of antidepressant use before, during, and after pregnancy: A systematic review and meta-analysis of timing, type of prescriptions and geographical variability. *J. Affect. Disord.* **264**, 82–89 (2020).
6. Robakis, T. K., Miyares, S. & Bergink, V. Risks and benefits of pre-delivery taper in pregnant women taking antidepressants. *Acta Psychiatr. Scand.* **150**, 355–359 (2023).
7. Wang, S. M. et al. Addressing the side effects of contemporary antidepressant drugs: a comprehensive review. *Chonnam Med. J.* **54**, 101–112 (2018).
8. Nezafati, M. H., Eshraghi, A., Vojdanparast, M., Abtahi, S. & Nezafati, P. Selective serotonin reuptake inhibitors and cardiovascular events: a systematic review. *J. Res. Med. Sci.* **21**, 66 (2016).
9. Chen, Y., Fan, Q., Liu, Y., Shi, Y. & Luo, H. Cardiovascular toxicity induced by SSRIs: analysis of spontaneous reports submitted to FAERS. *Psychiatry Res.* **326**, 115300 (2023).
10. Wang, J. & Cosci, F. Neonatal withdrawal syndrome following late in utero exposure to selective serotonin reuptake inhibitors: a systematic review and meta-analysis of observational studies. *Psychother. Psychosom.* **90**, 299–307 (2021).
11. Levinson-Castiel, R., Merlob, P., Linder, N., Sirota, L. & Klinger, G. Neonatal abstinence syndrome after in utero exposure to selective serotonin reuptake inhibitors in term infants. *Arch. Pediatrics Adolesc. Med.* **160**, 173–176 (2006).
12. Ornoy, A. & Koren, G. SSRIs and SNRIs (SRI) in pregnancy: effects on the course of pregnancy and the offspring: how far are we from having all the answers?. *Int. J. Mol. Sci.* **20**, 2370 (2019).
13. De Vries, C., Gadzhanova, S., Sykes, M. J., Ward, M. & Roughead, E. A systematic review and meta-analysis considering the risk for congenital heart defects of antidepressant classes and individual antidepressants. *Drug Saf.* **44**, 291–312 (2021).
14. Ewing, G., Tatarchuk, Y., Appleby, D., Schwartz, N. & Kim, D. Placental transfer of antidepressant medications: implications for postnatal adaptation syndrome. *Clin. Pharmacokinetics* **54**, 359–370 (2015).
15. Huang, J., Feng, Q., Wang, L. & Zhou, B. Human pluripotent stem cell-derived cardiac cells: application in disease modeling, cell therapy, and drug discovery. *Front. Cell Dev. Biol.* **9**, 655161 (2021).
16. Campostrini, G. et al. Generation, functional analysis and applications of isogenic three-dimensional self-aggregating cardiac microtissues from human pluripotent stem cells. *Nat. Protoc.* **16**, 2213–2256 (2021).
17. Drakhlis, L. et al. Human heart-forming organoids recapitulate early heart and foregut development. *Nat. Biotechnol.* **39**, 737–746 (2021).
18. Hofbauer, P. et al. Cardioids reveal self-organizing principles of human cardiogenesis. *Cell* **184**, 3299–3317 (2021).
19. Lian, X. et al. Directed cardiomyocyte differentiation from human pluripotent stem cells by modulating Wnt/ $\beta$ -catenin signaling under fully defined conditions. *Nat. Protoc.* **8**, 162–175 (2013).
20. Zhao, D., Lei, W. & Hu, S. Cardiac organoid—a promising perspective of preclinical model. *Stem Cell Res. Ther.* **12**, 1–10 (2021).
21. Hendrick, V. et al. Placental passage of antidepressant medications. *Am. J. Psychiatry* **160**, 993–996 (2003).
22. Nebigil, C. G., Etienne, N., Messaddeq, N. & Maroteaux, L. Serotonin is a novel survival factor of cardiomyocytes: mitochondria as a target of 5-HT<sub>2B</sub>-receptor signaling. *FASEB J.* **17**, 1373–1375 (2003).
23. Wang, Q. et al. 5-HTR3 and 5-HTR4 located on the mitochondrial membrane and functionally regulated mitochondrial functions. *Sci. Rep.* **6**, 37336 (2016).
24. Fanibunda, S. E. et al. Serotonin regulates mitochondrial biogenesis and function in rodent cortical neurons via the 5-HT<sub>2A</sub> receptor and SIRT1–PGC-1 $\alpha$  axis. *Proc. Natl. Acad. Sci.* **116**, 11028–11037 (2019).
25. Collins, H. M. et al. Rebound activation of 5-HT neurons following SSRI discontinuation. *Neuropsychopharmacology* **49**, 1–10 (2024).
26. Schoretsanitis, G. et al. Antidepressant transfer into amniotic fluid, umbilical cord blood & breast milk: a systematic review & combined analysis. *Prog. Neuro Psychopharmacol. Biol. Psychiatry* **107**, 110228 (2021).
27. Bérard, A. et al. First trimester exposure to paroxetine and risk of cardiac malformations in infants: the importance of dosage. *Birth Defects Res. Part B Dev. Reprod. Toxicol.* **80**, 18–27 (2007).
28. Bar-Oz, B. et al. Paroxetine and congenital malformations: meta-analysis and consideration of potential confounding factors. *Clin. Therapeutics* **29**, 918–926 (2007).
29. Bérard, A. et al. The risk of major cardiac malformations associated with paroxetine use during the first trimester of pregnancy: a systematic review and meta-analysis. *Br. J. Clin. Pharmacol.* **81**, 589–604 (2016).
30. Huang, Y. & Zhou, B. Mitochondrial dysfunction in cardiac diseases and therapeutic strategies. *Biomedicines* **11**, 1500 (2023).
31. Hermansanz-Agustín, P. & Enríquez, J. A. Generation of reactive oxygen species by mitochondria. *Antioxidants* **10**, 415 (2021).
32. Pohjoismäki, J. L. & Goffart, S. The role of mitochondria in cardiac development and protection. *Free Radic. Biol. Med.* **106**, 345–354 (2017).
33. Liang, M. Z., Ke, T. L. & Chen, L. Mitochondrial protein PGAM5 emerges as a new regulator in neurological diseases. *Front. Mol. Neurosci.* **14**, 730604 (2021).
34. Cheng, M. et al. PGAM5: a crucial role in mitochondrial dynamics and programmed cell death. *Eur. J. cell Biol.* **100**, 151144 (2021).
35. Zhou, H. et al. Inhibitory effect of melatonin on necroptosis via repressing the Ripk3-PGAM5-CypD-mPTP pathway attenuates cardiac microvascular ischemia–reperfusion injury. *J. Pineal Res.* **65**, e12503 (2018).
36. Crocini, C. & Gotthardt, M. Cardiac sarcomere mechanics in health and disease. *Biophys. Rev.* **13**, 637–652 (2021).
37. Gao, Y., Peng, L. & Zhao, C. MYH7 in cardiomyopathy and skeletal muscle myopathy. *Mol. Cell. Biochem.* **479**, 393–417 (2024).
38. Pusztaszeri, M. P., Seelentag, W. & Bosman, F. T. Immunohistochemical expression of endothelial markers CD31, CD34, von Willebrand factor, and Fli-1 in normal human tissues. *J. Histochem. Cytochem.* **54**, 385–395 (2006).
39. Boldrini, M. et al. Hippocampal angiogenesis and progenitor cell proliferation are increased with antidepressant use in major depression. *Biol. Psychiatry* **72**, 562–571 (2012).
40. Maingrette, F. et al. Psychological stress impairs ischemia-induced neovascularization: protective effect of fluoxetine. *Atherosclerosis* **241**, 569–578 (2015).
41. Arumugasaamy, N., Gudelsky, A., Hurley-Novatny, A., Kim, P. C. & Fisher, J. P. Model placental barrier phenotypic response to fluoxetine and sertraline: a comparative study. *Adv. Healthc. Mater.* **8**, 1900476 (2019).
42. Duim, S. N., Goumans, M. J. & Kruithof, B. P. *WT1 in cardiac development and disease*, 211–233 (Exon Publications, 2016).
43. Díaz del Moral, S. et al. Deletion of the wilms’ tumor suppressor gene in the cardiac troponin-T lineage reveals novel functions of WT1 in heart development. *Front. Cell Dev. Biol.* **9**, 683861 (2021).
44. Halperin, D. & Reber, G. Influence of antidepressants on hemostasis. *Dialogues Clin. Neurosci.* **9**, 47–59 (2007).
45. Laporte, S. et al. Bleeding risk under selective serotonin reuptake inhibitor (SSRI) antidepressants: a meta-analysis of observational studies. *Pharmacol. Res.* **118**, 19–32 (2017).
46. Fearon, U., Canavan, M., Biniecka, M. & Veale, D. J. Hypoxia, mitochondrial dysfunction and synovial invasiveness in rheumatoid arthritis. *Nat. Rev. Rheumatol.* **12**, 385–397 (2016).



47. Crocini, C. et al. Impact of ANKRD1 mutations associated with hypertrophic cardiomyopathy on contraction parameters of engineered heart tissue. *Basic Res. Cardiol.* **108**, 1–12 (2013).
48. Sheikh, F., Lyon, R. C. & Chen, J. Functions of myosin light chain-2 (MYL2) in cardiac muscle and disease. *Gene* **569**, 14–20 (2015).
49. BurrIDGE, P. et al. Chemically defined generation of human cardiomyocytes. *Nat. Methods* **11**, 855–860 (2014).
50. Valente, A., Maddalena, L., Robb, E., Moradi, F. & Stuart, J. A simple ImageJ macro tool for analyzing mitochondrial network morphology in mammalian cell culture. *Acta Histochem.* **119**, 315–326 (2017).
51. Stein, J. M. et al. Software tool for automatic quantification of sarcomere length and organization in fixed and live 2D and 3D muscle cell cultures in vitro. *Curr. Protoc.* **2**, e462 (2022).
52. Kim, D., Langmead, B. & Salzberg, S. L. HISAT: a fast spliced aligner with low memory requirements. *Nat. Methods* **12**, 357–360 (2015).
53. Anders, S., Pyl, P. T. & Huber, W. HTSeq—a Python framework to work with high-throughput sequencing data. *bioinformatics* **31**, 166–169 (2015).
54. Love, M. I., Huber, W. & Anders, S. Moderated estimation of fold change and dispersion for RNA-seq data with DESeq2. *Genome Biol.* **15**, 1–21 (2014).
55. Yu, G., Wang, L. G., Han, Y. & He, Q. Y. clusterProfiler: an R package for comparing biological themes among gene clusters. *Omics J. Integr. Biol.* **16**, 284–287 (2012).

## Acknowledgements

We would like to thank Rhonda Powell and Avery Herren from the Histology Core of the Clemson Light Imaging Facility for processing the histology of the organoids. We also thank Dr. Lika Drakhlis from Hannover Medical School for providing guidance on generating cardiac organoids. This work was supported by American Heart Association Career Development Award (18CDA34110128 to Q.L.), Startup Funding from Clemson University (Q.L.), SPARK-South Carolina Alzheimer's Disease Research Center (ARDC) Pilot Grant (Q.L.), NIH Pathway to Independence Award (HL133473-01A1 to H.W.), and was partially supported by the COBRE in Human Genetics (P20 GM139769 to Dr. Trudy F. C. Mackay and Dr. Robert R. H. Anholt) from the National Institute of General Medical Sciences.

## Author contributions

Conceptualization, Q.L.; Methodology, Q.L., Y.S., H.W., C.E.B., X.L., P.Z. and J.L.F.; Software, Y.S., H.W. and Q.L.; Validation, Y.S., H.W., C.E.B., X.L. and Q.L.; Formal Analysis, Y.S., C.E.B. and Q.L.; Investigation, Q.L., Y.S., S.R.M. and J.R.L.; Resources, S.R.M. and J.R.L.; Data Curation, Q.L. and

Y.S.; Writing—Original Draft Preparation, Y.S.; Writing—Review and Editing, Y.S., Q.L., S.C.S., J.R.L. and H.W.; Visualization, Y.S. and Q.L.; Supervision, Q.L.; Project Administration, Q.L.; Funding Acquisition, Q.L. and H.W. All authors have read and agreed to the published version of the manuscript.

## Competing interests

The authors declare no competing interests.

## Additional information

**Supplementary information** The online version contains supplementary material available at <https://doi.org/10.1038/s42003-025-08168-8>.

**Correspondence** and requests for materials should be addressed to Qing Liu.

**Peer review information** *Communications Biology* thanks the anonymous reviewers for their contribution to the peer review of this work. Primary Handling Editors: Ngan Huang and Dario Ummarino.

**Reprints and permissions information** is available at <http://www.nature.com/reprints>

**Publisher's note** Springer Nature remains neutral with regard to jurisdictional claims in published maps and institutional affiliations.

**Open Access** This article is licensed under a Creative Commons Attribution-NonCommercial-NoDerivatives 4.0 International License, which permits any non-commercial use, sharing, distribution and reproduction in any medium or format, as long as you give appropriate credit to the original author(s) and the source, provide a link to the Creative Commons licence, and indicate if you modified the licensed material. You do not have permission under this licence to share adapted material derived from this article or parts of it. The images or other third party material in this article are included in the article's Creative Commons licence, unless indicated otherwise in a credit line to the material. If material is not included in the article's Creative Commons licence and your intended use is not permitted by statutory regulation or exceeds the permitted use, you will need to obtain permission directly from the copyright holder. To view a copy of this licence, visit <http://creativecommons.org/licenses/by-nc-nd/4.0/>.

© The Author(s) 2025